Joint Carrier-Code Index Modulation Aided M-ary Differential Chaos Shift Keying System

Xiangming Cai, Weikai Xu, *Member, IEEE,* Francis C. M. Lau, *Fellow, IEEE,* Lin Wang, *Senior Member, IEEE*

***Abstract*—A joint carrier-code index modulation aided M-ary differential chaos shift keying (JCCIM-MDCSK) system is proposed in this paper. In the proposed JCCIM-MDCSK system, the carrier and code indices are used to transmit extra carrier and code index bits, respectively. Moreover, the modulating bits are input to multiple M-ary DCSK modulators, and the resultant signals are transmitted by the selected spreading codes and loaded into the active carriers. The benefit of the joint carrier-code index modulation is fully exploited so that the data rate and bit-error-rate (BER) performance of the JCCIM-MDCSK system are enhanced in contrast to its competitors. In order to estimate the carrier and code index bits successfully, an effective joint carrier-code index detection algorithm is proposed for the JCCIM-MDCSK system. In addition, the theoretical BER expressions of the JCCIM-MDCSK system are derived over additive white Gaussian noise (AWGN) and multipath Rayleigh fading channels. Finally, the BER performance of the JCCIM-MDCSK system is compared to other state-of-the-art IM-based non-coherent chaotic communication systems. It is shown that the JCCIM-MDCSK system can achieve better BER performance than its competitors.**

***Index Terms*—Chaotic communication, differential chaos shift keying (DCSK), joint carrier-code index modulation, bit error rate (BER).**

I. Introduction

Spread spectrum (SS) technique uses data-independent, random-like sequences to spread a narrow-band information signal over a wide frequency band. Chaotic signals characterized by the wideband property are naturally suitable for the spread-spectrum communication. Chaotic communication [1]–[3] using a chaotic signal as its carrier is capable of providing many advantages, including low probability of interception (LPI) and fading mitigation in time-varying channels [4]–[7]. As a popular non-coherent chaotic communication scheme, differential chaos shift keying (DCSK) [8] and its variants have been widely studied in many scenarios, such as power line communication [9], underwater acoustic communication [10], cooperative communication [11], multiple input multiple output system [12], analog network coding system [13], non-binary protograph low-density parity-check (LDPC) coded modulation system [14], two-way relay network-coded system [15], simultaneous wireless information and power transfer system [16], continuous mobility scenario [17], ultra-wideband (UWB) scenario [18] and so on.

However, the data rate, energy efficiency and spectral efficiency of the conventional DCSK system are inferior because half of the symbol duration is used to transmit the non-information-bearing reference signal. To address this drawback, a circle-constellation-based M-ary DCSK [19] system, which is an extended version of the quadrature chaotic shift keying (QCSK) [20], was proposed to enhance the data rate and energy efficiency. Then, by adjusting constellation parameters, an adaptive multiresolution M-ary DCSK system was proposed to achieve a more flexible BER performance [21]. A hierarchical technique was applied to a square-constellation-based M-DCSK (S-M-DCSK) [22] system, and a hierarchical S-M-DCSK [23] system using non-uniformly spaced distance constellation was proposed to meet different quality-of-service (QoS).

In order to avoid the use of long delay lines, a code-shifted DCSK (CS-DCSK) [24] system and its generalized version (GCS-DCSK) [25] were proposed, in which their reference and information-bearing signals are separated by different Walsh code sequences rather than time delay multiplexing. By combining chaotic signals and their Hilbert transforms with Walsh codes, the orthogonal multilevel DCSK (OM-DCSK) [26] system established many orthogonal information-bearing signals for improving the data rate. A noise-reduction DCSK (NR-DCSK) system was proposed in [27], where a moving average filter was applied to the reference and information-bearing signals to enhance system performance.

Index modulation (IM) techniques, which use the indices of different transmission entities to convey extra information bits, have been proposed as a promising solution for future wireless communications [28]–[30]. Specifically, the IM technique has been widely investigated in molecular communication [31], human body communication [32], orthogonal frequency division multiplexing (OFDM) spread spectrum communication [33], turbulence-free optical wireless communication [34], e-health Internet of thing (IoT) applications [35] and so forth. In addition, the achievable rate of the OFDM-IM system was studied in [36]. By integrating index modulation with a multi-carrier DCSK [37], the authors of [38] proposed a carrier-index DCSK (CI-DCSK) system, which utilizes the index of active carrier to carry additional information bits. To further increase the data rate and spectral efficiency, the CI-DCSK system was extended to its M-ary version (CI-MDCSK) [39]. As a new transmission dimension of index modulation, code index modulation (CIM) based on the spreading code was presented to increase the data rate without adding extra system

This work was supported in part by the National Natural Science Foundation of China under Grant No. 61671395 and 61871337.

Xiangming Cai, Weikai Xu and Lin Wang are with the Department of Information and Communication Engineering, Xiamen University, Xiamen, P. R. China. (e-mail: samson0102@qq.com; xweikai@xmu.edu.cn; wanglin@xmu.edu.cn).

Francis C. M. Lau is with the Department of Electronic and Information Engineering, Hong Kong Polytechnic University, Kowloon, Hong Kong, P. R. China. (e-mail: francis-cm.lau@polyu.edu.hk).

This article has been accepted for publication in a future issue of this journal, but has not been fully edited. Content may change prior to final publication. Citation information: DOI 10.1109/TVT.2020.3041927, IEEE Transactions on Vehicular Technology

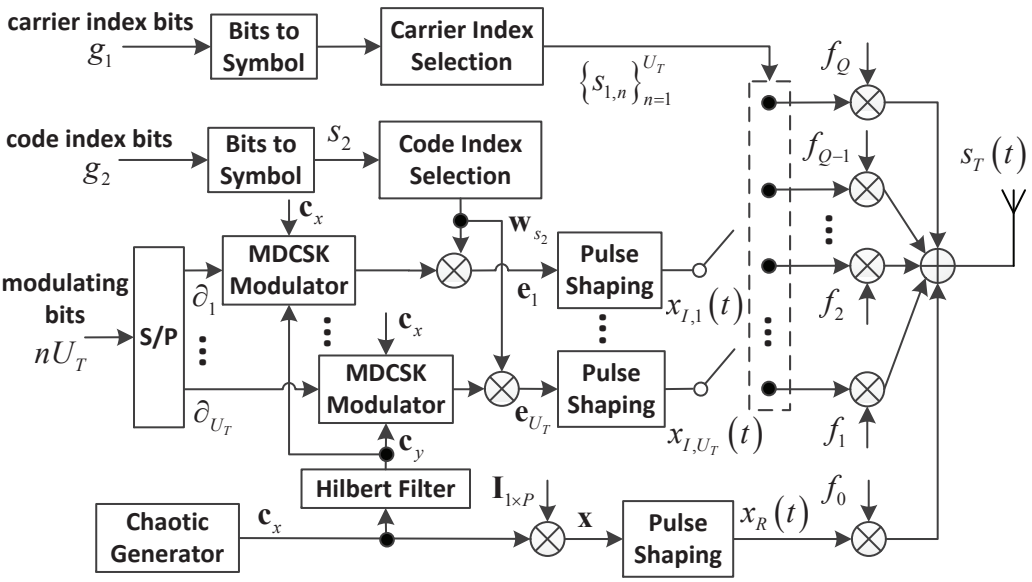

Fig. 1. Block diagram of the JCCIM-MDCSK transmitter.

complexity [40], [41]. Several works [42]–[44] have been done to obtain higher data rate and energy efficiency by combining the CIM technique with spatial modulation (SM). In [45], a short-reference DCSK with code index modulation (CIM-DCSK) was proposed, and then the noise-reduction and power coefficients optimization methods were applied to the CIM-DCSK system to further improve its BER performance.

Recently, a permutation index DCSK (PI-DCSK) [46] system was proposed with an aim to obtain higher energy efficiency without BER degradation compared to the OM-DCSK system. In this system, the reference signal is loaded into a permutation block to produce different permuted replicas, and then a permuted version is selected by the additional mapped bits. In a commutation code index DCSK (CCI-DCSK) [47] system, the reference signal along with its corresponding information-bearing signal determined by extra mapped bits are transmitted within the same time slot to enhance the spectral efficiency. A dual-mode DCSK with index modulation (DM-DCSK-IM) was proposed in [48], where the modulating bits are divided into two groups and used to modulate a pair of distinguishable modem-mode constellations. More recently, a multi-carrier M-ary DCSK with code index modulation (CIM-MC-MDCSK) was presented in [49], which not only inherits the low-complexity advantage of the MC-DCSK system, but also is capable of obtaining higher data rate and better BER performance. The authors of [50] proposed a joint index modulation system based on jointly driving the time and frequency of the signal to achieve better BER performance. A joint code-frequency IM (CFIM) scheme was proposed in [51] to meet the demand of low-power, low-complexity and inexpensive IoT devices. In addition, a two-dimensional spreading (time and frequency domain spreading) technique has been developed in the broadband orthogonal frequency and code division multiplexing (OFCDM) [52]–[54] system to achieve the high-rate data transmission.

Although many CIM-based and carrier-index DCSK systems are proposed in previous literature, these systems only provide an additional dimension (the spreading code index or carrier index) for information transmission. In this paper, a joint carrier-code index modulation aided M-ary differential chaos shift keying (JCCIM-MDCSK) system is proposed, where both carrier and code indices are used to transmit extra carrier and code index bits. Then, the modulating bits are input to multiple M-ary DCSK modulators. The resultant signals are spread by a selected Walsh code sequence and loaded into the active carriers. The proposed JCCIM-MDCSK system can obtain better data rate and BER performance than its competitors. Different from the CFIM scheme presented in [51], the proposed JCCIM-MDCSK system is a noncoherent scheme where the complicated channel estimation and equalization are avoided. Moreover, the number of activated carriers is more flexible in the JCCIM-MDCSK system, while the CFIM scheme only activates a carrier for information transmission so that the data rate of the CFIM system is limited. Although the OFCDM system uses the time and frequency domain spreading technique to improve the data rate, precise channel estimation is critical for the OFCDM system to realize hybrid detection [52]. In contrast, the proposed JCCIM-MDCSK system can combat the adverse effect of the multipath fading without the need for channel estimation. The main contributions of this paper are summarized as follows:

1) A joint carrier-code index modulation aided M-ary differential chaos shift keying system is proposed where the information bits are transmitted not only in the form of the modulating bits, but also the carrier index bits and code index bits.
2) To estimate the carrier and code index bits successfully, an efficient joint carrier-code index detection algorithm is proposed for the JCCIM-MDCSK system. After the carrier and code indices are determined, the modulating bits are recovered with the aid of M-ary DCSK demodulators.

3) The data rate, system complexity, energy efficiency and spectral efficiency of the JCCIM-MDCSK system are analyzed in detail. Compared to PI-DCSK, CIM-DCSK and CI-MDCSK systems, the JCCIM-MDCSK system obtains the largest data rate. However, the JCCIM-MDCSK system has lower spectral efficiency and energy efficiency than its competitors. In addition, the complexity of the JCCIM-MDCSK is higher than that of PI-DCSK and CI-MDCSK systems but much lower than the CIM-DCSK system.
4) The theoretical BER expressions of the JCCIM-MDCSK system are derived over AWGN and multipath Rayleigh fading channels. Then, the accuracy of our derivations are validated by simulations. The JCCIM-MDCSK system can obtain 1 to 3dB performance gain better than other DCSK-based systems, which demonstrates that the joint carrier-code index modulation performs better than one-dimension carrier index or code index modulation.

The remainder of this paper is organized as follows. Section II presents the system model of the JCCIM-MDCSK system, while Section III analyzes its data rate, system complexity, spectral efficiency and energy efficiency. The performance analysis of the JCCIM-MDCSK system is given in Section IV. Then, numerical results are shown in Section V. Section VI concludes this paper.

II. JCCIM-MDCSK System

A. The Transmitter

The block diagram of the JCCIM-MDCSK transmitter is shown in Fig. 1. In this configuration, there are $g = g_1 + g_2 + nU_T$ bits transmitted in a JCCIM-MDCSK symbol. Here, g_1 bits are carrier index bits used to select U_T active subcarriers out of Q available subcarriers, while g_2 bits are code index bits used to select a spreading code. In addition to this, nU_T modulating bits are arranged for physical transmission, in which every n bits are transmitted by an M-ary DCSK modulator and a selected subcarrier. Therefore, $g_1 = \lfloor \log_2 C_Q^{U_T} \rfloor$, where $C_Q^{U_T} = \frac{Q!}{U_T!(Q-U_T)!}$ denotes the total number of combinations and $\lfloor \cdot \rfloor$ is the floor function. In addition, $M = 2^n$ denotes the modulation order of the M-ary DCSK signal.

At the transmitter, the carrier index bits are firstly converted into the corresponding U_T active subcarrier indices $\{s_{1,u}\}_{u=1}^{U_T} \in \{1, 2, \cdots, Q\}$ via a k-combination mapping method [28], and the code index bits are transformed into the code index $s_2 \in \{1, 2, \cdots, P\}$, where $P = 2^{g_2}$ denotes the order of the Walsh code. Fig. 2 shows an example of the joint carrier-code index modulation with 4 available subcarriers (2 active subcarriers) and 8 Walsh codes.

Secondly, a logistic map $c_{k+1} = 1 - 2c_k^2, k = 1, 2, \cdots$ is employed in the chaotic generator to produce a length-θ chaotic signal $\mathbf{c}_x = [c_{x,1}, c_{x,2}, \cdots, c_{x,\theta}]$. Then the signal $\mathbf{c}_x$ is loaded into the Hilbert filter to obtain its orthogonal signal $\mathbf{c}_y$. The modulated symbol $\partial_u = (a_u, b_u), u = 1, 2, \cdots, U_T$ modulates $\mathbf{c}_x$ and $\mathbf{c}_y$ via the M-DCSK modulator and therefore $\mathbf{m}_u = a_u \mathbf{c}_x + b_u \mathbf{c}_y$. Fig. 3 gives an example for the QCSK and 8-ary DCSK constellations. After that, the M-DCSK signals $\mathbf{m}_u$ are spread by a selected P-length Walsh code sequence

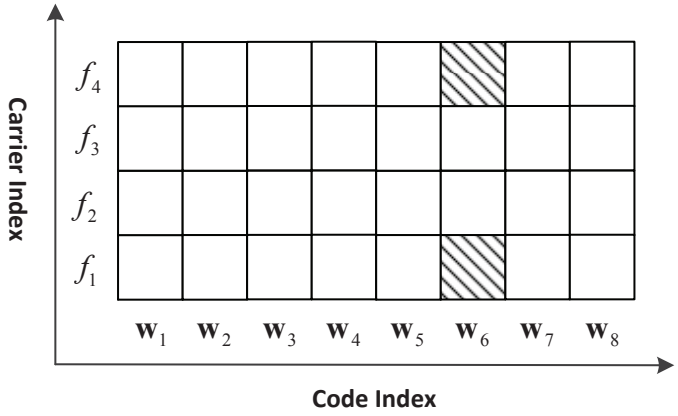

Fig. 2. An example of the joint carrier-code index modulation with 4 available carriers (2 active subcarrier) and 8 Walsh code sequences. The carrier and code index bits are 11 and 101, respectively. Then $2n$ modulating bits are input to 2 M-ary DCSK modulators. The resultant signals are spread by the selected Walsh code $\mathbf{w}_6$ and then transmitted by the 2 active subcarriers with frequencies f_1 and f_4.

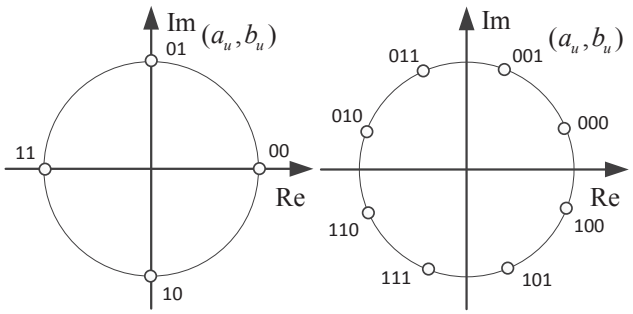

Fig. 3. An example for QCSK and 8-ary DCSK constellations.

$\mathbf{w}_{s_2} = [w_{s_2,1}, w_{s_2,2}, \cdots, w_{s_2,P}]$. Therefore, the information-bearing signals can be expressed by $\mathbf{e}_u = \mathbf{w}_{s_2} \otimes \mathbf{m}_u$, where $\otimes$ is the Kronecker product. The reference signal is given by $\mathbf{x} = \mathbf{I}_{1\times P} \otimes \mathbf{c}_\mathbf{x}$, where $\mathbf{I}_{1\times P}$ is a unit vector with length P.

Thirdly, the reference and multiple information-bearing signals are sent into the square-root raised-cosine pulse shaping filter $h_p(t)$. At the outputs of the pulse shaping blocks, the signals are given as $x_R(t) = \sum_{k=1}^{\beta} x_k h_p(t - kT_c)$ and $x_{I,u}(t) = \sum_{k=1}^{\beta} e_{u,k} h_p(t - kT_c)$, where x_k and $e_{u,k}$ denote the k^{th} element of x and e_u, respectively, T_c denotes the chip duration. The spreading factor of the JCCIM-MDCSK system is $\beta = P\theta$. Finally, the reference signal $x_R(t)$ is conveyed by the reference carrier with frequency f_0 and the M-ary information-bearing signals $x_{I,u}(t)$ are transmitted by the selected subcarriers with frequencies $f_{s_{1,u}}$. Therefore, the transmitted signal of the JCCIM-MDCSK system is given as

$$s_T(t) = x_R(t)\cos(2\pi f_0 t) + \sum_{u=1}^{U_T} x_{I,u}(t)\cos(2\pi f_{s_{1,u}} t). \quad (1)$$

In this paper, a time-invariant multipath Rayleigh fading channel $h(t) = \sum_{l=1}^{L} \lambda_l \delta(t - \tau_l)$ is considered, where L is the number of paths, λ_l and τ_l are the channel coefficient and the path delay corresponding to the l^{th} path. Assuming that the largest delay spread $\tau_{\max}$ is much less than the symbol

This article has been accepted for publication in a future issue of this journal, but has not been fully edited. Content may change prior to final publication. Citation information: DOI 10.1109/TVT.2020.3041927, IEEE Transactions on Vehicular Technology

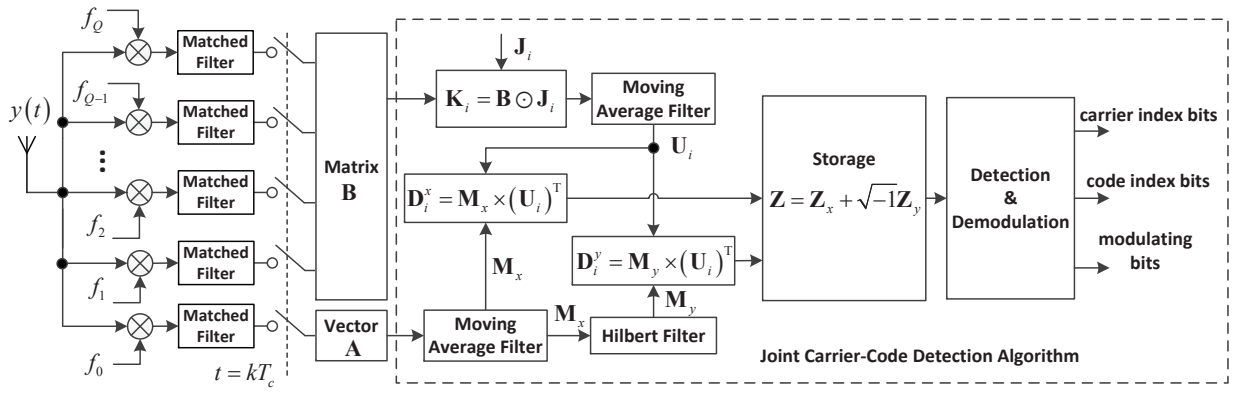

Fig. 4. Block diagram of the JCCIM-MDCSK receiver.

duration βT_c. Therefore, the orthogonality of both the Walsh code sequences and carriers is guaranteed. In this case, the received signal of the JCCI-MDCSK system is expressed as

$$y(t) = s_T(t) * h(t) + n(t), \tag{2}$$

where $*$ denotes the convolution operation and $n(t)$ is an AWGN with zero mean and $N_0/2$ variance.

B. The Receiver

Fig. 4 shows the block diagram of the JCCIM-MDCSK receiver. Assume that the carrier and Walsh codes are perfectly synchronized at the receiver. After the received signal is separated by different orthogonal carriers, the reference and information-bearing signals are obtained. Subsequently, these signals are processed by matched filters and sampled with interval T_c. Finally, the discrete outputs corresponding to the reference and information-bearing signals are stored in vector $\mathbf{A}$ and matrix $\mathbf{B}$, respectively, where $\mathbf{A}$ has one row and β columns and $\mathbf{B}$ has Q rows and β columns. Generally, the reference signal at the receiver is correlated with the information-bearing signals to demodulate the transmitted bits.

In order to restore the modulating bits, carrier index bits and code index bits, an effective joint carrier-code index detection algorithm is proposed for the JCCIM-MDCSK system. This joint detection algorithm is given in **Algorithm 1**. Firstly, the i^{th} Walsh code sequence $\mathbf{w}_i$ is spread as a matrix $\mathbf{J}_i$ with Q rows and β columns, i.e.,

$$\mathbf{J}_i = \begin{bmatrix} \mathbf{w}_i \otimes \mathbf{I}_{1\times\theta} \\ \mathbf{w}_i \otimes \mathbf{I}_{1\times\theta} \\ \vdots \\ \mathbf{w}_i \otimes \mathbf{I}_{1\times\theta} \end{bmatrix}_{Q\times\beta}, i = 1, 2, \cdots, P. \tag{3}$$

Afterwards, matrix $\mathbf{B}$ is multiplied by $\mathbf{J}_i$ using the Hadamard product $\odot$, i.e., $\mathbf{K}_i = \mathbf{B} \odot \mathbf{J}_i$. Besides, the discrete reference signal $\mathbf{A}$ can be represented as

$$\mathbf{A} = \left[\mathbf{Y}_1^R, \mathbf{Y}_2^R, \cdots, \mathbf{Y}_P^R\right]_{1\times\beta}, \tag{4}$$

where $\mathbf{Y}_j^R = [y_j^R(1), y_j^R(2), \cdots, y_j^R(\theta)], j = 1, 2, \cdots, P$. The vector $\mathbf{A}$ is further averaged using a moving average filter with a window size of P, namely

$$\begin{aligned} \mathbf{M}_x =& \frac{1}{P}\sum_{j=1}^{P}\mathbf{Y}_j^R \\ =& \frac{1}{P}\left[\sum_{j=1}^{P} y_j^R(1), \sum_{j=1}^{P} y_j^R(2), \cdots, \sum_{j=1}^{P} y_j^R(\theta)\right]_{1\times\theta}. \end{aligned} \tag{5}$$

Similarly, each row of $\mathbf{K}_i$ is averaged for every P elements to obtain

$$\mathbf{U}_i = \frac{1}{P}\begin{bmatrix} \sum_{k=1}^{P} y_{i,1,k}^I(1) & \cdots & \sum_{k=1}^{P} y_{i,1,k}^I(\theta) \\ \vdots & \ddots & \vdots \\ \sum_{k=1}^{P} y_{i,Q,k}^I(1) & \cdots & \sum_{k=1}^{P} y_{i,Q,k}^I(\theta) \end{bmatrix}_{Q\times\theta}, \tag{6}$$

where $i = 1, 2, \cdots, P$. $y_{i,Q,k}^I(\theta)$ is the θ^{th} element of the averaged information-bearing signal in the Q^{th} row and k^{th} subblock of matrix $\mathbf{K}_i$. The vector of the decision variable corresponding to the in-phase branch $\mathbf{D}_i^x, i = 1, 2, \cdots, P$ is

$$\begin{aligned} \mathbf{D}_i^x =& \mathbf{M}_x \times (\mathbf{U}_i)^{\mathrm{T}} \\ =& \frac{1}{P^2}\left[\sum_{j=1}^{P} y_j^R(1), \cdots, \sum_{j=1}^{P} y_j^R(\theta)\right] \times \\ & \begin{bmatrix} \sum_{k=1}^{P} y_{i,1,k}^I(1) & \cdots & \sum_{k=1}^{P} y_{i,1,k}^I(\theta) \\ \vdots & \ddots & \vdots \\ \sum_{k=1}^{P} y_{i,Q,k}^I(1) & \cdots & \sum_{k=1}^{P} y_{i,Q,k}^I(\theta) \end{bmatrix}^{\mathrm{T}} \\ =& \frac{1}{P^2}\left[\sum_{u=1}^{\theta}\left(\sum_{j=1}^{P} y_j^R(u)\sum_{k=1}^{P} y_{i,1,k}^I(u)\right), \cdots, \right. \\ & \left. \sum_{u=1}^{\theta}\left(\sum_{j=1}^{P} y_j^R(u)\sum_{k=1}^{P} y_{i,Q,k}^I(u)\right)\right]_{1\times Q}, \end{aligned} \tag{7}$$

where $(\cdot)^{\mathrm{T}}$ is the transposition operation. Thus the matrix of the in-phase branch $\mathbf{Z}_x$ can be expressed by (8), as shown at the bottom of this page. Besides, the matrix of the quadrature

This article has been accepted for publication in a future issue of this journal, but has not been fully edited. Content may change prior to final publication. Citation information: DOI 10.1109/TVT.2020.3041927, IEEE Transactions on Vehicular Technology

branch $\mathbf{Z}_y$ can be obtained in a similar manner. Therefore, $\mathbf{Z} = \mathbf{Z}_x + \sqrt{-1}\mathbf{Z}_y$.

Subsequently, the receiver finds the U_T maximum values from all elements of $\|\mathbf{Z}\|_2$, where $\|\cdot\|_2$ denotes the squared Frobenius norm of a matrix. For simplicity, define

$$\begin{aligned} Z_{\psi,\xi} =& \frac{1}{P^2}\sum_{u=1}^{\theta}\left(\sum_{j=1}^{P} y_j^R(u)\sum_{k=1}^{P} y_{\psi,\xi,k}^I(u)\right) \\ &+ \sqrt{-1}\frac{1}{P^2}\sum_{u=1}^{\theta}\left(\sum_{j=1}^{P} \tilde{y}_j^R(u)\sum_{k=1}^{P} y_{\psi,\xi,k}^I(u)\right), \end{aligned} \tag{9}$$

where the signal $\tilde{y}_j^R(u)$ obtained from the output of the Hilbert filter is orthogonal to the reference signal $y_j^R(u)$. In addition, $\psi = 1, 2, \cdots, P$ and $\xi = 1, 2, \cdots, Q$ denote the element in the ψ^{th} row and ξ^{th} column of the matrix $\mathbf{Z}$. Finally, the code and carrier indices are estimated by finding the U_T largest absolute values of $Z_{\psi,\xi}$, described as

$$\left(\hat{\psi}, \hat{\xi}_i\right) = \arg \max_{\psi\in\aleph_1, \xi\in\aleph_2} \{|Z_{\psi,\xi}|\}, i = 1, 2, \cdots, U_T \tag{10}$$

where $\hat{\psi}$ and $\{\hat{\xi}_i\}_{i=1}^{U_T}$ denote an estimated code index and U_T estimated carrier indices, respectively. $\aleph_1 = \{1, 2, \cdots, P\}$ and $\aleph_2 = \{1, 2, \cdots, Q\}$ are all possible code and carrier indices, respectively. By estimating the selected code and active carrier indices $\hat{\psi}$ and $\hat{\xi}_i, i = 1, 2, \ldots, U_T$, the JCCIM-MDCSK receiver is capable of recovering the code index bits and carrier index bits, respectively. After the code and carrier indices are determined, the modulating bits are easily estimated via the use of M-DCSK demodulators.

Algorithm 1 Joint Carrier-Code Index Detection Algorithm

Initialization

1: The discrete reference and information-bearing signals are stored in vector $\mathbf{A}$ and matrix $\mathbf{B}$, respectively.
2: The i^{th} Walsh code sequence $\mathbf{w}_i$ is spread as a matrix $\mathbf{J}_i$.

Averaging

1: Multiply matrix $\mathbf{B}$ by $\mathbf{J}_i$ using Hadamard product $\odot$ and yield $\mathbf{K}_i = \mathbf{B} \odot \mathbf{J}_i$.
2: Vector $\mathbf{A}$ and each row of $\mathbf{K}_i$ are averaged for every P elements to obtain $\mathbf{M}_x$ and $\mathbf{U}_i$.
3: Signal $\mathbf{M}_x$ is loaded into the Hilbert filter to obtain its orthogonal signal $\mathbf{M}_y$.

Correlation

1: Multiply $\mathbf{M}_x$ by $(\mathbf{U}_i)^{\mathrm{T}}$ to obtain $\mathbf{D}_i^x = \mathbf{M}_x \times (\mathbf{U}_i)^{\mathrm{T}}$. Similarly, $\mathbf{D}_i^y = \mathbf{M}_y \times (\mathbf{U}_i)^{\mathrm{T}}$.
2: By storing $\mathbf{D}_i^x + \sqrt{-1}\mathbf{D}_i^y$ into the matrix $\mathbf{Z}$, all possible decision variables are obtained.

Search

1: Find the U_T maximum values from all elements of $\|\mathbf{Z}\|_2$. The code and carrier indices are estimated as $\hat{\psi}$ and $\hat{\xi}_i, i = 1, 2, \cdots, U_T$.

Recovery

1: After converting $\hat{\psi}$ and $\hat{\xi}_i$ into binary numbers, the code and carrier index bits are restored.
2: The modulating bits are estimated via the use of M-DCSK demodulators.

III. Data Rate, System Complexity, Spectral Efficiency and Energy Efficiency Analysis

In this subsection, the data rate, complexity, spectral efficiency and energy efficiency of the JCCIM-MDCSK system are analyzed and then compared to PI-DCSK, CIM-DCSK and CI-MDCSK systems. Generally, the data rate is defined as the total number of transmitted bits per symbol. In the proposed JCCIM-MDCSK system, both carrier and code indices are used to transmit the additional mapped bits. The overall number of the transmitted bits per symbol is given as $\kappa_1 = \lfloor \log_2 C_Q^{U_T} \rfloor + \log_2 P + nU_T$. As a matter of fact, in the JCCIM-MDCSK system, one out of all possible Walsh code sequences is selected to spread the multiple M-ary information-bearing signals and U_T out of Q subcarriers are activated to transmit the obtained signals. In contrast, the permutation operation in the PI-DCSK system only provides a dimension for extra information transmission, and the data rate of this system equals $\kappa_2 = \log_2 M_p + 1$, where M_p is the overall number of permutation operations. Furthermore, the CIM-DCSK system only uses the dimension of spreading codes to carry the additional mapped bits. Therefore, its data rate is given as $\kappa_3 = \log_2 P + 1$. Regarding the CI-MDCSK system, only one dimension (active carrier index) is used to transmit the extra information bits. Thus the data rate of the CI-MDCSK system is stated as $\kappa_4 = \log_2 Q + n$. Table I shows the data rates of JCCIM-MDCSK, PI-DCSK, CIM-DCSK and CI-MDCSK systems. Moreover, the data rate of the conventional DCSK system is listed for reference. The JCCIM-MDCSK system is capable of transmitting more bits than its competitors with the help of the joint carrier-code index modulation. In addition, the data rate of the JCCIM-MDCSK system can be further enhanced via adjusting the modulation order of the M-ary DCSK and increasing the

$$\mathbf{Z}_x = \begin{bmatrix} \mathbf{D}_1^x \\ \mathbf{D}_2^x \\ \vdots \\ \mathbf{D}_P^x \end{bmatrix} = \frac{1}{P^2}\begin{bmatrix} \sum_{u=1}^{\theta}\left(\sum_{j=1}^{P} y_j^R(u)\sum_{k=1}^{P} y_{1,1,k}^I(u)\right) & \cdots & \sum_{u=1}^{\theta}\left(\sum_{j=1}^{P} y_j^R(u)\sum_{k=1}^{P} y_{1,Q,k}^I(u)\right) \\ \vdots & \ddots & \vdots \\ \sum_{u=1}^{\theta}\left(\sum_{j=1}^{P} y_j^R(u)\sum_{k=1}^{P} y_{P,1,k}^I(u)\right) & \cdots & \sum_{u=1}^{\theta}\left(\sum_{j=1}^{P} y_j^R(u)\sum_{k=1}^{P} y_{P,Q,k}^I(u)\right) \end{bmatrix}_{P\times Q}. \tag{8}$$

This article has been accepted for publication in a future issue of this journal, but has not been fully edited. Content may change prior to final publication. Citation information: DOI 10.1109/TVT.2020.3041927, IEEE Transactions on Vehicular Technology

TABLE I
COMPARISONS OF DATA RATE, SYSTEM COMPLEXITY, SPECTRAL EFFICIENCY AND ENERGY EFFICIENCY

System	Data Rate	Complexity	Spectral Efficiency	Energy Efficiency
JCCIM-MDCSK	$\lfloor \log_2 C_Q^{U_T} \rfloor + \log_2 P + nU_T$	$(U_T + 2PQ)\, P\theta + \sum_{i=0}^{U_T-1} C_{PQ-i}^1$	$\frac{\lfloor \log_2 C_Q^{U_T} \rfloor + \log_2 P + nU_T}{(1+Q)\Omega P \theta T_c}$	$\frac{\lfloor \log_2 C_Q^{U_T} \rfloor + \log_2 P + nU_T}{(1+U_T) P \sum_{k=1}^{\theta} c_k^2}$
PI-DCSK	$\log_2 M_p + 1$	$(1 + M_p)\theta + C_{M_p}^1$	$\frac{\log_2 M_p + 1}{2\theta T_c \Omega}$	$\frac{\log_2 M_p + 1}{2 \sum_{k=1}^{\theta} c_k^2}$
CIM-DCSK	$\log_2 P + 1$	$(1 + P)^2\theta + C_P^1$	$\frac{\log_2 P + 1}{(1+P)\theta T_c \Omega}$	$\frac{\log_2 P + 1}{(1+P) \sum_{k=1}^{\theta} c_k^2}$
CI-MDCSK	$\log_2 Q + n$	$(1 + 2Q)\, \theta + C_Q^1$	$\frac{\log_2 Q + n}{(1+Q)\Omega \theta T_c}$	$\frac{\log_2 Q + n}{2 \sum_{k=1}^{\theta} c_k^2}$
DCSK	1	2θ	$\frac{1}{2\theta T_c \Omega}$	$\frac{1}{2 \sum_{k=1}^{\theta} c_k^2}$

overall number of active subcarriers. Clearly, the data rate of the JCCIM-MDCSK system is higher than that of other chaotic communication systems.

In this paper, the number of multiplications used for spreading/despreading operations is applied to evaluate the system complexity. The searching complexity of code or/and carrier indices is also considered as a part of system complexity. At the JCCIM-MDCSK transmitter, only one out of P spreading codes is selected to spread the M-ary information-bearing signals and then the resultant signals are transmitted by the U_T active subcarriers selected from Q subcarriers. Therefore, U_T spreading operations are needed at the JCCIM-MDCSK transmitter. At the JCCIM-MDCSK receiver, in order to find the U_T active subcarriers and the selected spreading code, PQ despreading operations are needed in the in-phase branch of the M-ary DCSK demodulator. In addition, since the JCCIM-MDCSK receiver needs to find the U_T largest absolute values of $Z_{\psi,\xi}$ to obtain the Walsh code and carrier indices, the searching complexity of the joint code-carrier indices is $\sum_{i=0}^{U_T-1} C_{PQ-i}^1$. Therefore, the complexity of the JCCIM-MDCSK system is $\mathcal{O}_1 = (U_T + 2PQ)P\theta + \sum_{i=0}^{U_T-1} C_{PQ-i}^1$. The PI-DCSK system needs M_p despreading operation in its receiver and its searching complexity is $C_{M_p}^1$, therefore the complexity of the PI-DCSK system is $\mathcal{O}_2 = (1 + M_p)\theta + C_{M_p}^1$. The CIM-DCSK system only needs P despreading operations at its receiver and its searching complexity is C_P^1. As for the CI-MDCSK system, Q despreading operations are needed in the in-phase branch of the M-ary DCSK demodulator. Moreover, the searching complexity of the CI-MDCSK system is C_Q^1. Consequently, the complexities of CIM-DCSK and CI-MDCSK systems are $\mathcal{O}_3 = (1 + P)^2\theta + C_P^1$ and $\mathcal{O}_4 = (1 + 2Q)\theta + C_Q^1$, respectively. Table I shows the system complexity of the JCCIM-MDCSK and other chaotic communication systems. For a more straightforward comparison, the complexity of different systems is plotted in Fig. 5. The total data rate of all systems is equal to 5. In the JCCIM-MDCSK system, $P = 2$, $Q = 2$, $U_T = 1$ and $M = 8$. Moreover, $M_p = 16$ and $P = 16$ are used in PI-DCSK and CIM-DCSK systems, respectively. In the CI-MDCSK system, $Q = 4$ and $M = 8$. As shown in Fig. 5, the complexity of the JCCIM-MDCSK system is higher than that of PI-DCSK and CI-MDCSK systems but much lower than the CIM-DCSK system.

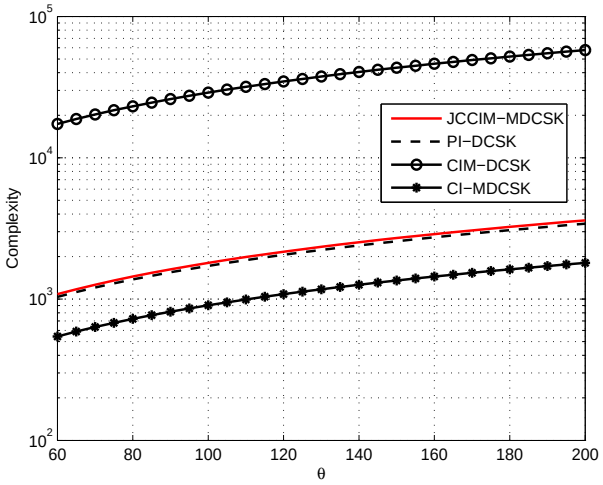

Fig. 5. The complexity comparison between JCCIM-MDCSK and other IM-based DCSK systems with the same data rate.

Table I shows the spectral efficiency of the JCCIM-MDCSK and other DCSK-based systems. Generally, the spectral efficiency is defined as the ratio of bit rate to total bandwidth in bits/s/Hz. It is assumed that the bandwidth of subcarrier in all systems is equal to Ω. Since the proposed JCCIM-MDCSK uses multiple carriers for data transmission, its spectral efficiency is lower than its competitors. In addition, the energy efficiency of different DCSK-based systems is also given in Table I. Clearly, the total number of transmitted bits per energy can be used as an indicator for energy efficiency. Therefore, the energy efficiency can be obtained by performing the reciprocal operation of bit energy. When $U_T = 1$ and $P = 2$, the energy efficiency of the JCCIM-MDCSK system is $\frac{\frac{1}{2}(\lfloor \log_2 Q \rfloor + n + 1)}{2 \sum_{k=1}^{\theta} c_k^2}$, which is inferior to that of the CI-MDCSK system.

IV. PERFORMANCE ANALYSIS

In our proposed JCCIM-MDCSK system, there are $g = g_1 + g_2 + nU_T$ bits transmitted in a symbol, where g_1 carrier index bits and g_2 code index bits are applied to select U_T active subcarriers and a spreading code. These $g_1 + g_2$ bits are referred to as mapped bits used to determine the combination

This article has been accepted for publication in a future issue of this journal, but has not been fully edited. Content may change prior to final publication. Citation information: DOI 10.1109/TVT.2020.3041927, IEEE Transactions on Vehicular Technology

of the active subcarriers and a selected Walsh code. The remaining nU_T bits are termed as modulating bits which are modulated into U_T M-ary information-bearing signals for physical transmission. In this configuration, the BER of the JCCIM-MDCSK system is composed of the BER of the modulating bits P_{mod} and the BER of the mapped bits P_{map} with weight coefficients $\frac{nU_T}{g_1+g_2+nU_T}$ and $\frac{g_1+g_2}{g_1+g_2+nU_T}$, respectively. Therefore, the overall bit error probability of the JCCIM-MDCSK system is given by

$$P_{sys} = \frac{nU_T}{g_1+g_2+nU_T} P_{mod} + \frac{g_1+g_2}{g_1+g_2+nU_T} P_{map}. \quad (11)$$

The BER of modulating bits is determined by the probability of the erroneous joint carrier-code index detection P_{ccim} and the BER of the M-ary DCSK P_e. More explicitly, the BER of the modulating bits is generated by two different scenarios. In the first scenario, the joint carrier-code index detection is correct but the modulating bits have probability P_e being demodulated incorrectly. In the second scenario, the joint carrier-code index is detected incorrectly and the modulating bits are therefore estimated using the incorrect joint carrier-code index. Under this condition, the receiver has to guess the modulating bits with probability P_g, where P_g denotes the average BER of the modulating bits on the misjudged subcarriers and is given by

$$P_g = \frac{\sum_{i=1}^{U_T} C_{U_T}^i \left[\frac{i}{2} + P_e\left(U_T - i\right)\right]}{U_T \sum_{i=1}^{U_T} C_{U_T}^i}. \quad (12)$$

Hence, the overall BER of modulating bits is obtained as

$$P_{mod} = \left(1 - P_{ccim}\right) P_e + P_g P_{ccim}, \quad (13)$$

The bit error probability of the mapped bits is associated with the BER of the joint carrier-code index detection P_{ccim}. When the joint carrier-code index is detected incorrectly, it will result in an entirely different combination of mapped bits. Since the frequencies of carriers and the spreading Walsh codes are independent of each other, the relationship of P_{map} and P_{ccim} can be described as

$$P_{map} = \frac{2^{(g_1+g_2-1)}}{2^{(g_1+g_2)}-1} P_{ccim}. \quad (14)$$

Substituting (13) and (14) into (11), the BER of the JCCIM-MDCSK system can be rewritten as

$$\begin{aligned} P_{sys} =& \frac{1}{g_1+g_2+nU_T}[nU_T((1-P_{ccim})P_e + P_g P_{ccim}) \\ &+ \frac{2^{(g_1+g_2-1)}}{2^{(g_1+g_2)}-1}(g_1+g_2)P_{ccim}]. \end{aligned} \quad (15)$$

1) Bit Error Probability of M-ary DCSK P_e: Since the M-ary information-bearing signals carried by all active subcarriers are independent of each other and they have same error probability, we only need to evaluate one of them. Assuming the p^{th} Walsh code sequence is selected to spread the M-ary information-bearing signal and then the q^{th}, $q \in \{\hat{\xi}_i\}_{i=1}^{U_T}$ carrier is activated to carry the resultant spread signal. When the joint carrier-code index detection is correct, the decision variable of the in-phase branch $Z_{p,q}^x$ from the joint carrier-code correlation block is expressed as

$$Z_{p,q}^x = \frac{1}{P^2} \sum_{u=1}^{\theta} \left(\sum_{j=1}^{P} y_j^R(u) \sum_{k=1}^{P} y_{p,q,k}^I(u) \right). \quad (16)$$

Here, $\frac{1}{P}\sum_{j=1}^{P} y_j^R(u)$ denotes the reference signal processed by the averaging filter and is represented as

$$\begin{aligned} \frac{1}{P}\sum_{j=1}^{P} y_j^R(u) =& \frac{1}{P}\sum_{j=1}^{P}\sum_{l=1}^{L} \lambda_l c_{(j-1)\theta+u-\tau_l}^x + \frac{1}{P}\sum_{j=1}^{P} n_{(j-1)\theta+u}^R \\ =& \sum_{l=1}^{L} \lambda_l c_{u-\tau_l}^x + n_u^R, \end{aligned} \quad (17)$$

where n_u^R denotes the averaged additive white Gaussian noise added in the reference signal and its mean and variance are zero and $N_0/(2P)$, respectively. Similarly, the averaged information-bearing signal $\frac{1}{P}\sum_{k=1}^{P} y_{p,q,k}^I(u)$ is given as

$$\frac{1}{P}\sum_{k=1}^{P} y_{p,q,k}^I(u) = \sum_{l=1}^{L} \lambda_l \left(a_i c_{u-\tau_l}^x + b_i c_{u-\tau_l}^y\right) + n_u^I, \quad (18)$$

where n_u^I is the averaged additive white Gaussian noise in the received information-bearing signal with the same mean and variance as n_u^R. Therefore, the decision variable $Z_{p,q}^x$ can be rewritten as (19), as shown at the bottom of this page. The mean and variance of $Z_{p,q}^x$ can be calculated by

$$\mathrm{E}\left[Z_{p,q}^x\right] = \sum_{l=1}^{L} \lambda_l^2 \frac{a_i E_s}{P\left(1+U_T\right)} = a_i E_m, \quad (20)$$

$$\mathrm{Var}\left[Z_{p,q}^x\right] = \sum_{l=1}^{L} \lambda_l^2 \frac{E_s N_0}{\left(1+U_T\right)P^2} + \theta\frac{N_0^2}{4P^2} = \sigma_1^2, \quad (21)$$

where $E_s = (1+U_T)P\theta\mathrm{E}[c_{u-\tau_l}^2]$ is the symbol energy of the JCCIM-MDCSK system and $E_m = \sum_{l=1}^{L}\lambda_l^2 \frac{E_s}{P(1+U_T)}$. Similarly, the mean and variance of decision variable $Z_{p,q}^y$ corresponding to the quadrature branch can be obtained as

$$\mathrm{E}\left[Z_{p,q}^y\right] = \sum_{l=1}^{L} \lambda_l^2 \frac{b_i E_s}{P\left(1+U_T\right)} = b_i E_m, \quad (22)$$

$$\begin{aligned} Z_{p,q}^x =& \sum_{u=1}^{\theta} \left(\sum_{l=1}^{L} \lambda_l c_{u-\tau_l}^x + n_u^R \right) \left(\sum_{l=1}^{L} \lambda_l \left(a_i c_{u-\tau_l}^x + b_i c_{u-\tau_l}^y\right) + n_u^I \right) \\ =& \sum_{u=1}^{\theta} \left(\sum_{l=1}^{L} \lambda_l^2 a_i \left(c_{u-\tau_l}^x\right)^2 + \sum_{l=1}^{L} \lambda_l^2 b_i c_{u-\tau_l}^x c_{u-\tau_l}^y + \sum_{l=1}^{L} \lambda_l c_{u-\tau_l}^x n_u^I + \sum_{l=1}^{L} \lambda_l \left(a_i c_{u-\tau_l}^x + b_i c_{u-\tau_l}^y\right) n_u^R + n_u^R n_u^I \right). \end{aligned} \quad (19)$$

$$\mathrm{Var}\left[Z_{p,q}^{y}\right]=\sum_{l=1}^{L}\lambda_l^2\frac{E_sN_0}{\left(1+U_T\right)P^2}+\theta\frac{N_0^2}{4P^2}=\sigma_1^2, \quad (23)$$

At the receiver, the M-ary DCSK demodulator is used to estimate the modulating bits. Therefore, the bit error probability P_e is given by [55]

$$P_e\approx\frac{2}{n}Q_f\left(\frac{\rho\pi}{M}\right), M>2 \quad (24)$$

where $Q_f(x)=\frac{1}{\sqrt{2\pi}}\int_x^{+\infty}\exp(-\frac{t^2}{2})\mathrm{d}t, x\geq 0$, $\rho=\frac{E_m}{\sigma_1}=\frac{2\gamma_s}{\sqrt{4(1+U_T)\gamma_s+\theta(1+U_T)^2}}$, γ_s is the symbol-SNR given as $\gamma_s=\sum_{l=1}^{L}\lambda_l^2\frac{E_s}{N_0}$. When $M=2$,

$$\begin{aligned}P_e\approx&\frac{1}{2}\mathrm{erfc}\left[\left(\frac{2\mathrm{Var}\left[Z_{p,q}^{x}\right]}{\left(\mathrm{E}\left[Z_{p,q}^{x}\right]\right)^2}\right)^{-\frac{1}{2}}\right]\\=&\frac{1}{2}\mathrm{erfc}\left[\left(\frac{2(1+U_T)}{\gamma_s}+\frac{\theta(1+U_T)^2}{2\gamma_s^2}\right)^{-\frac{1}{2}}\right],\end{aligned} \quad (25)$$

where $\mathrm{erfc}(x)=\frac{2}{\sqrt{\pi}}\int_x^{\infty}e^{-t^2}\mathrm{d}t$ denotes the complementary error function.

2) Erroneous Joint Carrier-Code Index Detection Probability P_{ccim}: When the joint carrier-code index detection is incorrect, the decision variable of the in-phase branch $Z_{\psi,\xi}^{x}$ $\psi\neq p$ or $\xi\neq q$, $q\in\{\hat{\xi}_i\}_{i=1}^{U_T}$ is expressed as

$$Z_{\psi,\xi}^{x}=\sum_{u=1}^{\theta}\left[\left(\sum_{l=1}^{L}\lambda_l c_{u-\tau_l}^{x}+n_u^R\right)n_u^I\right]. \quad (26)$$

Therefore, the mean and variance of $Z_{\psi,\xi}^{x}$ are computed as

$$\mathrm{E}\left[Z_{\psi,\xi}^{x}\right]=0, \quad (27)$$

$$\mathrm{Var}\left[Z_{\psi,\xi}^{x}\right]=\sum_{l=1}^{L}\lambda_l^2\frac{E_sN_0}{2\left(1+U_T\right)P^2}+\theta\frac{N_0^2}{4P^2}=\sigma_2^2. \quad (28)$$

The mean and variance of the decision variable $Z_{\psi,\xi}^{y}$ corresponding to the quadrature branch can be obtained in a similar manner, i.e., $\mathrm{E}[Z_{\psi,\xi}^{y}]=0$ and $\mathrm{Var}[Z_{\psi,\xi}^{y}]=\sigma_2^2$.

To estimate the joint carrier-code index, the JCCIM-MDCSK receiver needs to find the U_T maximum absolute values from the output of all correlators. When the joint carrier-code index detection is correct, the mean and variance of the decision variable $Z_{p,q}=Z_{p,q}^{x}+\sqrt{-1}Z_{p,q}^{y}$ are $\mathrm{E}[Z_{p,q}]=\mathrm{E}[Z_{p,q}^{x}]+\mathrm{E}[Z_{p,q}^{y}]=(a_i+b_i)E_m$ and $\mathrm{Var}[Z_{p,q}]=\mathrm{Var}[Z_{p,q}^{x}]+\mathrm{Var}[Z_{p,q}^{y}]=2\sigma_1^2$, respectively. When the joint carrier-code index detection is incorrect, the mean and variance of decision variable $Z_{\psi,\xi}=Z_{\psi,\xi}^{x}+\sqrt{-1}Z_{\psi,\xi}^{y}$ are given as $\mathrm{E}[Z_{\psi,\xi}]=\mathrm{E}[Z_{\psi,\xi}^{x}]+\mathrm{E}[Z_{\psi,\xi}^{y}]=0$ and $\mathrm{Var}[Z_{\psi,\xi}]=\mathrm{Var}[Z_{\psi,\xi}^{x}]+\mathrm{Var}[Z_{\psi,\xi}^{y}]=2\sigma_2^2$. The estimation is correct when the minimum absolute values of the decision variables $Z_{p,q}$ corresponding to the p^{th} selected Walsh code sequence and the q^{th}, $q\in\{\hat{\xi}_i\}_{i=1}^{U_T}$ active carrier is greater than the maximum absolute values of the decision variables $Z_{\psi,\xi}$, ($\psi\neq p$ or $\xi\neq q$) for any inactive carriers and non-selected Walsh codes. Let $Z_{\min}=\min(|Z_{p,q}|), q\in\{\hat{\xi}_i\}_{i=1}^{U_T}$. When equiprobable transmission is considered, the probability of the erroneous joint carrier-code index detection P_{ccim} can be obtained as

$$\begin{aligned}P_{ccim}=&1-P\left\{Z_{\min}>\max\left(|Z_{\psi,\xi}|\right)|\psi\neq p,\xi\neq q\right\}\\=&1-\int_0^{\infty}F_{\max(|Z_{\psi,\xi}|)}\left(t\right)f_{Z_{\min}}\left(t\right)\mathrm{d}t\\=&1-\int_0^{\infty}\left[F_{|Z_{\psi,\xi}|}\left(t\right)\right]^{P+Q-U_T}f_{Z_{\min}}\left(t\right)\mathrm{d}t,\end{aligned} \quad (29)$$

where $F_{|Z_{\psi,\xi}|}(t)$ is the cumulative distribution function (CDF) of $|Z_{\psi,\xi}|$. In addition, $f_{|Z_{p,q}|}(t)$ is the probability density function (PDF) of $|Z_{p,q}|$. The decision variables $Z_{p,q}$ and $Z_{\psi,\xi}$ can be regarded as Gaussian variables, and thus their absolute values $|Z_{p,q}|$ and $|Z_{\psi,\xi}|$ follow a folded normal distribution. Note that the U_T decision variables $|Z_{p,q}|, q\in\{\hat{\xi}_i\}_{i=1}^{U_T}$ are independent of each other and they have the same mean and variance. The CDF of $Z_{\min}$ is therefore given by

$$F_{Z_{\min}}(t)=1-\left[1-F_{|Z_{p,q}|}(t)\right]^{U_T}. \quad (30)$$

The PDF of $Z_{\min}$ can be obtained after performing the differentiation operation on $F_{Z_{\min}}(t)$, namely

$$f_{Z_{\min}}(t)=U_T\left[1-F_{|Z_{p,q}|}(t)\right]^{U_T-1}f_{|Z_{p,q}|}(t) \quad (31)$$

where $F_{|Z_{p,q}|}(t)=\frac{1}{2}[\mathrm{erf}(\frac{t-(a_i+b_i)E_m}{\sqrt{2(2\sigma_1^2)}})+\mathrm{erf}(\frac{t+(a_i+b_i)E_m}{\sqrt{2(2\sigma_1^2)}})]$, $f_{|Z_{p,q}|}(t)=\frac{1}{\sqrt{2\pi(2\sigma_1^2)}}\{e^{-\frac{[t-(a_i+b_i)E_m]^2}{2(2\sigma_1^2)}}+e^{-\frac{[t+(a_i+b_i)E_m]^2}{2(2\sigma_1^2)}}\}$ and $F_{|Z_{\psi,\xi}|}(t)=\mathrm{erf}(\frac{t}{\sqrt{2(2\sigma_2^2)}})$. Furthermore, $\mathrm{erf}(x)=\frac{2}{\sqrt{\pi}}\int_0^x e^{-t^2}\mathrm{d}t, x\geq 0$ is the error function. Finally, the erroneous joint carrier-code index detection probability P_{ccim} is obtained as

$$\begin{aligned}P_{ccim}=&1-\frac{1}{\sqrt{2\pi\left(2\sigma_1^2\right)}}\int_0^{\infty}\left[\mathrm{erf}\left(\frac{t}{\sqrt{2\left(2\sigma_2^2\right)}}\right)\right]^{P+Q-U_T}\\&\times U_T\left\{1-\frac{1}{2}\left[\mathrm{erf}\left(\frac{t-\left(a_i+b_i\right)E_m}{\sqrt{2\left(2\sigma_1^2\right)}}\right)\right.\right.\\&\left.\left.+\mathrm{erf}\left(\frac{t+\left(a_i+b_i\right)E_m}{\sqrt{2\left(2\sigma_1^2\right)}}\right)\right]\right\}^{U_T-1}\\&\times\left\{e^{-\frac{\left[t-\left(a_i+b_i\right)E_m\right]^2}{2\left(2\sigma_1^2\right)}}+e^{-\frac{\left[t+\left(a_i+b_i\right)E_m\right]^2}{2\left(2\sigma_1^2\right)}}\right\}\mathrm{d}t.\end{aligned} \quad (32)$$

3) BER of JCCIM-MDCSK system P_{sys}: According to the above analysis, the BER expression of the JCCIM-MDCSK system is obtained by putting (24) or (25) and (32) into (15). In this paper, it is assumed that all paths in the multipath Rayleigh fading channels are independent of each other and they have the same channel gain. Under this condition, the PDF of γ_s is given by [56]

$$f\left(\gamma_s\right)=\frac{\gamma_s^{L-1}}{(L-1)!\bar{\gamma}_l^{L}}\exp\left(-\frac{\gamma_s}{\bar{\gamma}_l}\right), \quad (33)$$

where $\bar{\gamma}_l=\frac{E_s}{N_0}\mathrm{E}[\lambda_i^2]=\frac{E_s}{N_0}\mathrm{E}[\lambda_j^2], i\neq j$ denotes the average instantaneous SNR measured in the l^{th} channel. Finally, the averaged BER of the JCCIM-MDCSK system over the multipath Rayleigh fading channel is obtained by $\bar{P}_{sys}=\int_0^{\infty}P_{sys}\cdot f(\gamma_s)\mathrm{d}\gamma_s$, namely (34), as shown at the

This article has been accepted for publication in a future issue of this journal, but has not been fully edited. Content may change prior to final publication. Citation information: DOI 10.1109/TVT.2020.3041927, IEEE Transactions on Vehicular Technology

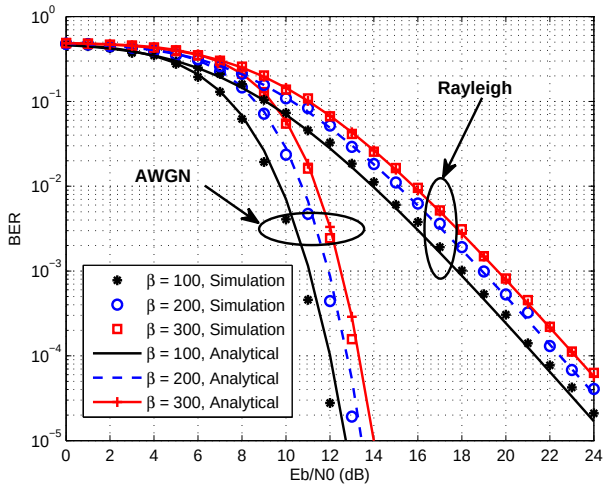

Fig. 6. BER performance of the JCCIM-MDCSK system with different spreading factors over AWGN and multipath Rayleigh fading channels. $P = 2$, $Q = 8$, $U_T = 1$ and $M = 2$.

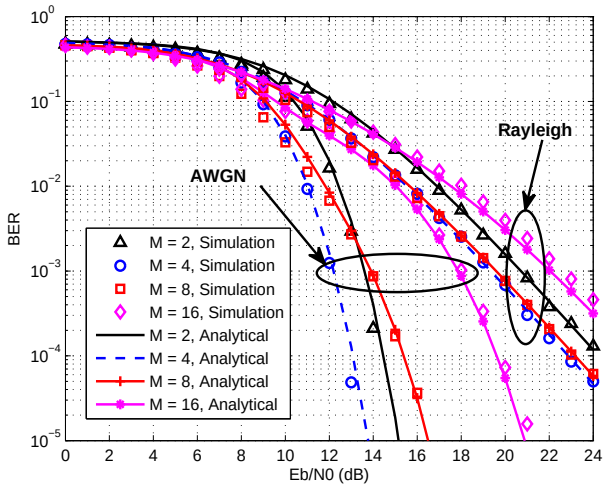

Fig. 7. BER performance of the JCCIM-MDCSK system with various modulation orders over AWGN and multipath Rayleigh fading channels. $\beta = 200$, $P = 2$, $Q = 4$ and $U_T = 2$.

bottom of this page. Although a closed-form expression is not given, Eq. (34) can be calculated by the simple numerical integration. Note that when $L = 1$, an unit channel coefficient $\lambda_1 = 1$ and zero time delay $\tau_1 = 0$ are considered, the channel degrades into an AWGN channel.

V. Numerical Results

A. BER Performance Evaluation

Fig. 6 shows the BER performance of the JCCIM-MDCSK system with different spreading factors over AWGN and multipath Rayleigh fading channels. Unless otherwise stated, a three-path Rayleigh fading channel with the same average power gains and time delays $\tau_1 = 0, \tau_2 = 2, \tau_3 = 4$ is used in our simulations. As observed in Fig. 6, the simulation results are in good agreement with the analytical results, and they confirm our theoretical derivations. Moreover, it is clearly shown that the BER performance of the JCCIM-MDCSK system is deteriorated when the spreading factor increases from 100 to 300. When the spreading factor increases, the noise component involved in noise-noise correlation term becomes more significant, resulting in a poor BER performance.

The BER performance of the JCCIM-MDCSK system with various modulation orders is given in Fig. 7. Clearly, the simulation results match the corresponding theoretical ones. As observed, the JCCIM-MDCSK system with $M = 4$ performs better than other cases in an AWGN channel. The JCCIM-MDCSK system with $M = 8$ shows similar BER performance compared to $M = 4$ in a multipath Rayleigh fading channel, which is about 1dB performance gain over $M = 2$ at a BER level 10^{-3}. In addition, the influence of U_T on the BER performance of the JCCIM-MDCSK system

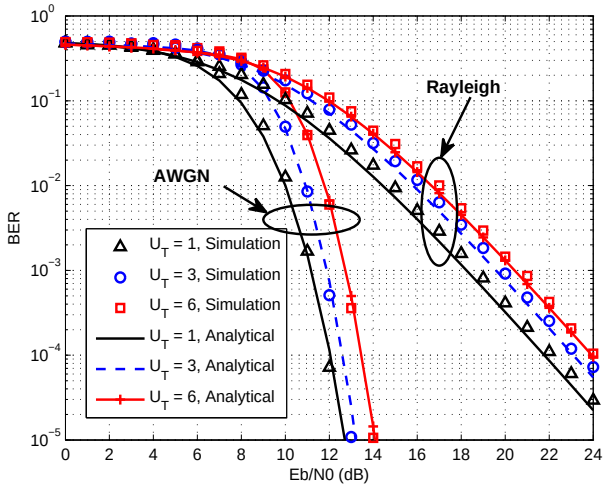

Fig. 8. BER performance of the JCCIM-MDCSK system with various U_T over AWGN and multipath Rayleigh fading channels. $\beta = 200$, $P = 2$, $Q = 8$ and $M = 4$.

is shown in Fig. 8. It is observed that the JCCIM-MDCSK system with $U_T = 1$ obtains about 1.5dB gain over $U_T = 6$ in an AWGN channel at a BER of 10^{-3}. Regarding the multipath Rayleigh fading channel, the BER performance of the JCCIM-MDCSK system with $U_T = 1$ has about 2dB gain over that of $U_T = 6$ at a BER level 10^{-3}. It is mainly because the error probability of carrier detection increases when the number of active carriers U_T increases, thereby worsening the overall BER performance of the JCCIM-MDCSK system.

Fig. 9 investigates the influence of the number of carrier index bits g_1 on the BER performance of the JCCIM-MDCSK

$$\bar{P}_{sys} = \int_0^{\infty} \frac{1}{g_1 + g_2 + nU_T} \left[nU_T \left((1 - P_{ccim}) P_e + P_g P_{ccim} \right) + \frac{2^{(g_1+g_2-1)}}{2^{(g_1+g_2)} - 1} (g_1 + g_2) P_{ccim} \right] \cdot f(\gamma_s) \mathrm{d}\gamma_s. \quad (34)$$

This article has been accepted for publication in a future issue of this journal, but has not been fully edited. Content may change prior to final publication. Citation information: DOI 10.1109/TVT.2020.3041927, IEEE Transactions on Vehicular Technology

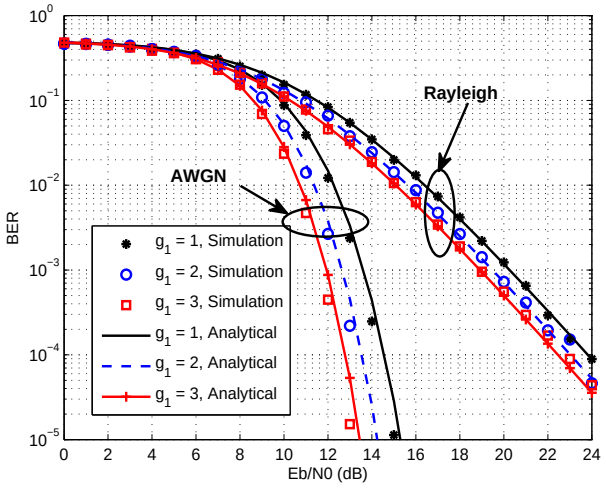

Fig. 9. BER performance of the JCCIM-MDCSK system over AWGN and multipath Rayleigh fading channels. $\beta = 200$, $P = 2$, $M = 2$, $U_T = 1$ and $g_1 = 1, 2, 3$, namely $Q = 2, 4, 8$.

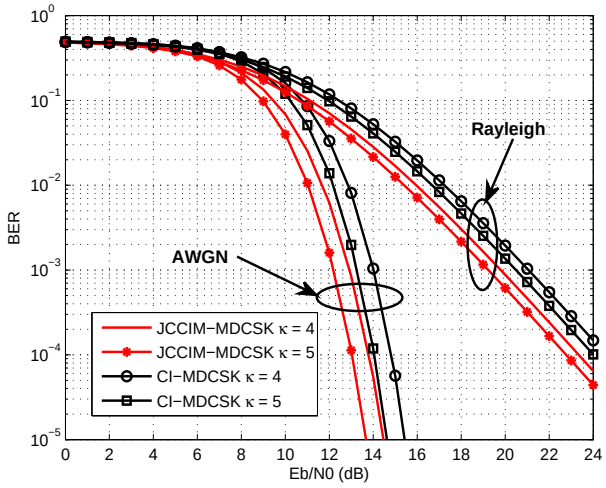

Fig. 11. BER performance comparison of JCCIM-MDCSK and CI-MDCSK systems with $\beta = 240$, $\kappa = 4, 5$ over AWGN and multipath Rayleigh fading channels.

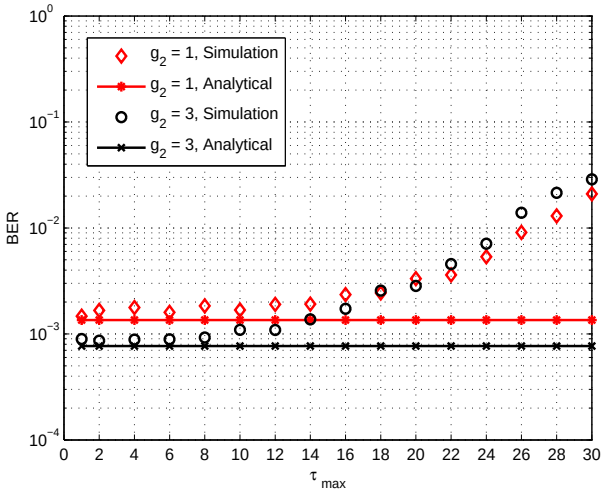

Fig. 10. The effect of the maximum delay $\tau_{\max}$ on the BER performance of the JCCIM-MDCSK system with $\theta = 50$ and $E_b/N_0 = 22$dB over a two-path Rayleigh fading channel with equal channel gains.

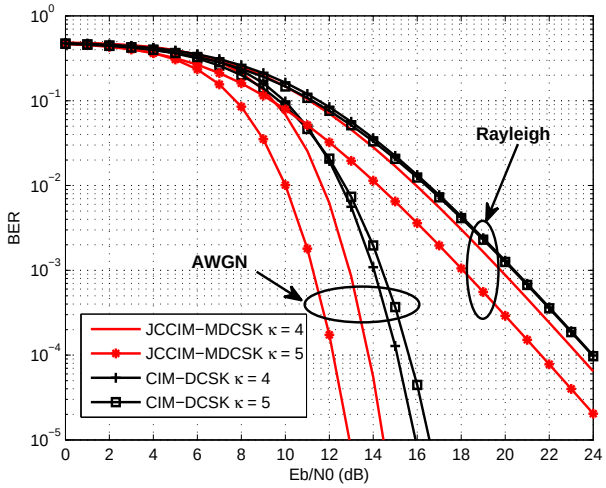

Fig. 12. BER performance comparison of JCCIM-MDCSK and CIM-DCSK systems with $\beta = 480$, $\kappa = 4, 5$ over AWGN and multipath Rayleigh fading channels.

system. The theoretical results match the simulation results. Fig. 9 indicates that the BER performance of the JCCIM-MDCSK system is improved when g_1 increases. Explicitly, in order to achieve a BER of 10^{-5}, the required E_b/N_0 for the JCCIM-MDCSK system with $g_1 = 1$ is almost 2dB higher than $g_1 = 3$. It is because in the case of same transmitted energy, more carrier index bits are mapped within a symbol which means the required E_b/N_0 to achieve a certain BER is reduced. More specifically, the carrier index bits are transmitted implicitly by the status of whether the carrier is activated or not, and therefore these bits can be conveyed without the consumption of transmitted energy. More carrier index bits mean that the energy used for the modulating bits is increased, therefore improving the BER performance. As shown in Fig. 6–9, the proposed JCCIM-MDCSK system can achieve a better BER performance when $M = 4$, $U_T = 1$, β is small and g_1 is large in contrast to other cases.

The influence of the maximum delay $\tau_{\max}$ on the BER performance of the JCCIM-MDCSK system is given in Fig. 10. In our simulation, $Q = 2$, $U_T = 1$, $M = 2$ and $P = 2, 8$ are used in the JCCIM-MDCSK system, therefore $g_1 = 1$ and $g_2 = 1, 3$. A two-path Rayleigh fading channel with equal channel gains is used. When the maximum delay $\tau_{\max}$ is small ($\tau_{\max} \ll \beta$), the inter-symbol interference (ISI) can be neglected. Therefore, the simulated results match the theoretical ones. However, as $\tau_{\max}$ increases, the effect of ISI becomes more significant and thus causes a deteriorating BER performance in the JCCIM-MDCSK system.

B. BER Performance Comparison

The BER performance of the JCCIM-MDCSK system in contrast to the CI-MDCSK system is evaluated in Fig. 11.

This article has been accepted for publication in a future issue of this journal, but has not been fully edited. Content may change prior to final publication. Citation information: DOI 10.1109/TVT.2020.3041927, IEEE Transactions on Vehicular Technology

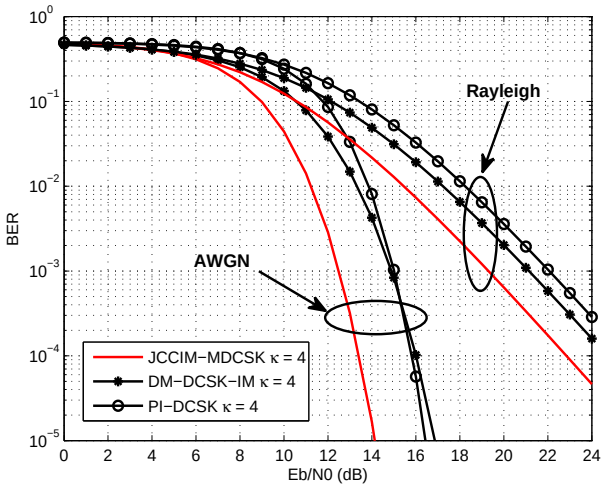

Fig. 13. BER performance comparison of JCCIM-MDCSK and other chaotic communication systems with the same number of transmitted bits per symbol over AWGN and multipath Rayleigh fading channels.

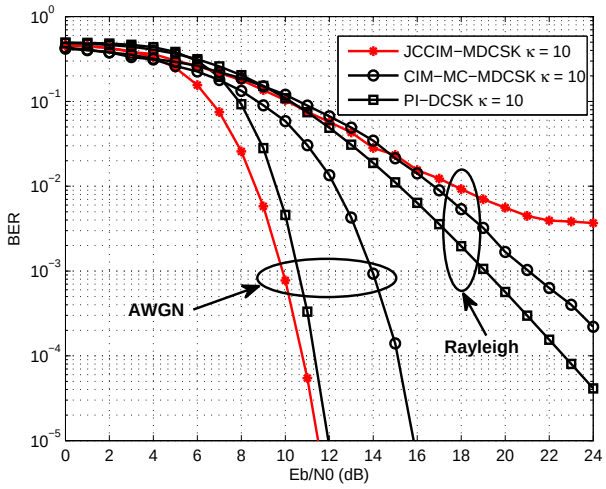

Fig. 14. BER performance comparison of JCCIM-MDCSK, CIM-MC-MDCSK and PI-DCSK systems over AWGN and multipath Rayleigh fading channels with large delays.

$Q = 4, 8$, $U_T = 1$, $M = 2$ and $P = 2$ are used in the simulation of the JCCIM-MDCSK system. Note that the spreading factor and modulation order are the same for JCCIM-MDCSK and CI-MDCSK systems. In addition, the total number of transmitted bits per symbol is $\kappa = 4, 5$. It is observed that the proposed JCCIM-MDCSK system outperforms the CI-MDCSK system over both AWGN and multipath Rayleigh fading channels. For example, the JCCIM-MDCSK system achieves about 1dB performance gain over the CI-MDCSK system at a BER level 10^{-5} when $\kappa = 4$. Fig. 12 shows the BER performance of JCCIM-MDCSK and CIM-DCSK systems. In the JCCIM-MDCSK simulation, the simulation parameters are set to $P = 4, 8$, $M = 2$, $Q = 2$ and $U_T = 1$. The JCCIM-MDCSK system obtains better BER performance than the CIM-DCSK system. For instance, in the AWGN channel, when $\kappa = 4$, the performance improvement of the JCCIM-MDCSK system over the CIM-DCSK system is more than 1.5dB at a BER level of 10^{-5}. Furthermore, the performance gain is greater than 3dB when $\kappa = 5$ at the same BER level. The above comparisons demonstrate that the JCCIM-MDCSK system is capable of providing better BER performance than CI-MDCSK and CIM-DCSK systems.

As shown in Fig. 13, in order to highlight the superiority of the JCCIM-MDCSK system, the BER performance of the JCCIM-MDCSK system is compared with that of DM-DCSK-IM and PI-DCSK systems. The overall number of transmitted bits per symbol for JCCIM-MDCSK, DM-DCSK-IM and PI-DCSK systems are equal to 4, namely $\kappa = 4$. The spreading factor is $\beta = 360$ for all the systems. Moreover, $P = 4$, $M = 2$, $Q = 2$ and $U_T = 1$ are applied in the JCCIM-MDCSK simulation. Since the multiple carriers and Walsh codes are used to transmit the information bits in the JCCIM-MDCSK system, the overall bandwidth of the JCCIM-MDCSK system is much higher than other single-carrier DCSK-based systems (such as DM-DCSK-IM and PI-DCSK systems). In an AWGN channel, the JCCIM-MDCSK system achieves more than 2dB performance gain in contrast to the PI-DCSK system at the BER level of 10^{-5}. In a multipath Rayleigh fading channel, the JCCIM-MDCSK system can obtain approximate 2dB performance gain compared to the DM-DCSK-IM system at a BER level of 10^{-3}. Therefore, the JCCIM-MDCSK system possesses a higher resistance against the fading channel than other non-coherent chaotic communication systems and thus this system is suitable for the rugged environment of future wireless communication.

In Fig. 14, the BER performance of the JCCIM-MDCSK system is compared to that of CIM-MC-MDCSK and PI-DCSK systems under the condition of large delays. Note that a three-path Rayleigh fading channel with unequal channel coefficients $\mathrm{E}\left[\lambda_1^2\right] = 6/10, \mathrm{E}\left[\lambda_2^2\right] = 3/10, \mathrm{E}\left[\lambda_3^2\right] = 1/10$ and time delay $\tau_1 = 0, \tau_2 = 3, \tau_3 = 20$ is used in our simulations. Moreover, the overall number of transmitted bits per symbol is 10 for all systems (i.e., $\kappa = 10$). $P = 4$, $M = 2$ and $\beta = 400$ are used in the simulations of JCCIM-MDCSK and CIM-MC-MDCSK systems. Other parameters for the JCCIM-MDCSK system are $Q = 8$ and $U_T = 2$. As shown in Fig. 14, the JCCIM-MDCSK system can obtain more than 4dB gain than the CIM-MC-MDCSK system in the AWGN channel. However, in the multipath Rayleigh fading channel, the JCCIM-MDCSK system reaches to its error floor more quickly compared to the CIM-MC-MDCSK system. Therefore, the JCCIM-MDCSK shows weaker robustness against the fading channel with large multipath delays.

Finally, Fig. 15 studies the BER performance of JCCIM-MDCSK, CI-MDCSK and PI-DCSK systems on the condition of different complexity for index detection. Here, the complexity of index detection is defined as the searching complexity of code or/and carrier indices, represented by ϖ. According to Section IV, the complexities of index detection for JCCIM-MDCSK, CI-MDCSK and PI-DCSK systems are $\sum_{i=0}^{U_T-1} C_{PQ-i}^1$, C_Q^1 and $C_{M_p}^1$, respectively. In the JCCIM-MDCSK system, $P = 2$, $U_T = 1$ and $M = 2$. In addition, the

This article has been accepted for publication in a future issue of this journal, but has not been fully edited. Content may change prior to final publication. Citation information: DOI 10.1109/TVT.2020.3041927, IEEE Transactions on Vehicular Technology

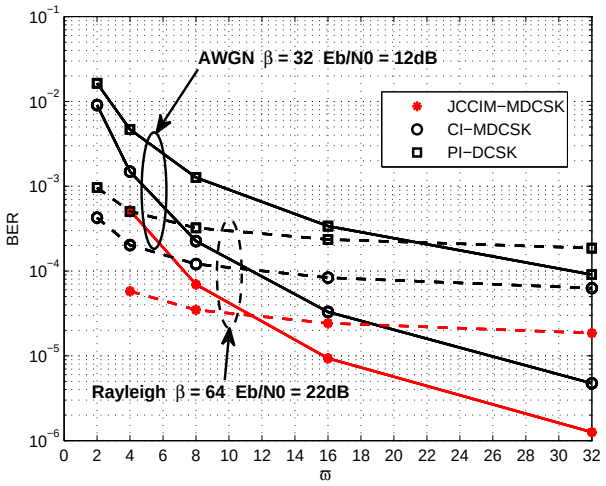

Fig. 15. BER performance comparison of JCCIM-MDCSK, CI-MDCSK and PI-DCSK systems on the condition of different complexity for index detection over AWGN and multipath Rayleigh fading channels.

CI-MDCSK system uses $M = 2$ in its simulation. As shown in Fig. 15, with the increase of ϖ, the BER performance of all systems is improved. The main reason is that when the complexity of index detection increases, more carrier index bits or code index bits are additionally transmitted within a symbol, thus enhancing the system performance. Moreover, the JCCIM-MDCSK system outperforms CI-MDCSK and PI-DCSK systems for different ϖ.

VI. Conclusions

The joint carrier-code index modulation aided M-ary differential chaos shift keying system has been proposed in this paper. This design obtains the benefits of both carrier index modulation and code index modulation. In the JCCIM-MDCSK system, the information bits are conveyed not only in the form of the physically modulating bits but also the carrier index bits as well as code index bits. By exploiting carrier and code indices to transmit additional information bits, the proposed JCCIM-MDCSK system is capable of achieving superior BER performance in comparison with its competitors. The data rate, system complexity, energy efficiency and spectral efficiency of the JCCIM-MDCSK system are compared to PI-DCSK, CIM-DCSK, CI-MDCSK and DCSK systems. It is indicated that the JCCIM-MDCSK system can obtain the highest data rate. However, the spectral efficiency and energy efficiency are lower than its competitors. In addition, the complexity of the proposed JCCIM-MDCSK system is higher than that of PI-DCSK and CI-MDCSK systems but much lower than the CIM-DCSK system.

Furthermore, the analytical BER expressions of the JCCIM-MDCSK system have been derived over AWGN and multipath Rayleigh fading channels. Finally, the BER performance of the JCCIM-MDCSK system is compared with CI-MDCSK, CIM-DCSK, DM-DCSK-IM, PI-DCSK and CIM-MC-MDCSK systems. The obtained results show that the JCCIM-MDCSK system possesses a strong robustness in the rugged environment. Specifically, the JCCIM-MDCSK system can obtain 1 to 3dB performance gain in contrast to other DCSK-based systems, which demonstrates that the joint carrier-code index modulation performs better than one-dimension carrier index or code index modulation. However, when a multipath channel with large delays is considered, the BER performance of the JCCIM-MDCSK system reaches to the error floor more quickly compared to CIM-MC-MDCSK and PI-DCSK systems. In addition, the JCCIM-MDCSK system outperforms CI-MDCSK and PI-DCSK systems on the condition of different complexity for index detection. Since the orthogonal spreading codes have been widely used in the code division multiple access (CDMA), the JCCIM-MDCSK system can be extended to the multiuser communication scenario. Moreover, the closed-form theoretical expressions of IM-based DCSK systems have not been fully investigated, and therefore this will be our future research direction.

References

[1] F. C. M. Lau and C. K. Tse, *Chaos-Based Digital Communication Systems: Operating Principles, Analysis Methods, and Performance Evaluation*. Berlin, Germany: Springer-Verlag, 2003.

[2] G. Kaddoum, "Wireless chaos-based communication systems: A comprehensive survey," *IEEE Access*, vol. 4, pp. 2621-2648, 2016.

[3] Y. Fang, G. Han, P. Chen, F. C. M. Lau, G. Chen, and L. Wang, "A survey on DCSK-based communication systems and their application to UWB scenarios," *IEEE Commun. Surveys Tuts.*, vol. 18, no. 3, pp. 1804-1837, Third Quarter 2016.

[4] J. Yu and Y.-D. Yao, "Detection performance of chaotic spreading LPI waveforms," *IEEE Trans. Wireless Commun.*, vol. 4, no. 2, pp. 390-396, Mar. 2005.

[5] Y. Xia, C. K. Tse, and F. C. M. Lau, "Performance of differential chaos shift-keying digital communication systems over a multipath fading channel with delay spread," *IEEE Trans. Circuits Syst. II, Exp. Briefs*, vol. 51, no. 12, pp. 680-684, Dec. 2004.

[6] M. Dawa, G. Kaddoum and Z. Sattar, "A generalized lower bound on the bit error rate of DCSK systems over multi-path rayleigh fading channels," *IEEE Trans. Circuits Syst. II, Exp. Briefs*, vol. 65, no. 3, pp. 321-325, March 2018.

[7] M. Dawa, G. Kaddoum and M. Herceg, "A framework for the lower bound on the BER of DCSK systems over multi-path Nakagami-m fading channels," *IEEE Trans. Circuits Syst. II, Exp. Briefs*. doi: 10.1109/TCSII.2019.2950529.

[8] G. Kolumbán, G. K. Vizvári, W. Schwarz, and A. Abel, "Differential chaos shift keying: A robust coding for chaos communication," in *Proc. Nonlinear Dyn. Electron. Syst.*, Seville, Spain, 1996, pp. 92-97.

[9] G. Kaddoum and N. Tadayon, "Differential chaos shift keying: A robust modulation scheme for power-line communications," *IEEE Trans. Circuits Syst. II, Exp. Briefs*, vol. 64, no. 1, pp. 31-35, Jan. 2017.

[10] M. Chen, W. Xu, D. Wang and L. Wang, "Multi-carrier chaotic communication scheme for underwater acoustic communications," *IET Commun.*, vol. 13, no. 14, pp. 2097-2105, 27 8 2019.

[11] W. Xu, L. Wang and G. Chen, "Performance of DCSK cooperative communication systems over multipath fading channels," *IEEE Trans. Circuits Syst. I, Reg. Papers*, vol. 58, no. 1, pp. 196-204, Jan. 2011.

[12] Y. Fang, J. Xu, L. Wang, and G. Chen, "Performance of MIMO relay DCSK-CD systems over Nakagami fading channels," *IEEE Trans. Circuits Syst. I, Reg. Papers*, vol. 60, no. 3, pp. 757-767, Mar. 2013.

[13] G. Kaddoum and F. Shokraneh, "Analog network coding for multi-user multi-carrier differential chaos shift keying communication system," *IEEE Trans. Wireless Commun.*, vol. 14, no. 3, pp. 1492-1505, Mar. 2015.

[14] P. Chen, L. Shi, Y. Fang, G. Cai, L. Wang and G. Chen, "A coded DCSK modulation system over Rayleigh fading channels," *IEEE Trans. Commun.*, vol. 66, no. 9, pp. 3930-3942, Sept. 2018.

[15] G. Cai, Y. Fang, G. Han, J. Xu, and G. Chen, "Design and analysis of relay-selection strategies for two-way relay network-coded DCSK systems," *IEEE Trans. Veh. Technol.*, vol. 67, no. 2, pp. 1258-1271, Feb. 2018.

[16] G. Kaddoum, H. V. Tran, L. Kong, and M. Atallah, "Design of simultaneous wireless information and power transfer scheme for short reference DCSK communication systems," *IEEE Trans. Commun.*, vol. 65, no. 1, pp. 431-443, Jan. 2017.

[17] F. J. Escribano, G. Kaddoum, A. Wagemakers, and P. Giard, "Design of a new differential chaos-shift-keying system for continuous mobility," *IEEE Trans. Commun.*, vol. 64, no. 5, pp. 2066-2078, May 2016.

[18] L. Wang, X. Min, and G. Chen, "Performance of SIMO FM-DCSK UWB system based on chaotic pulse cluster signals," *IEEE Trans. Circuits Syst. I, Reg. Papers*, vol. 58, no. 9, pp. 2259-2268, Apr. 2011.

[19] L. Wang, G. Cai and G. R. Chen, "Design and performance analysis of a new multiresolution M-ary differential chaos shift keying communication system," *IEEE Trans. Wireless Commun.*, vol. 14, no. 9, pp. 5197-5208, Sept. 2015.

[20] Z. Galias and G. M. Maggio, "Quadrature chaos-shift keying: Theory and performance analysis," *IEEE Trans. Circuits Syst. I, Fundam. Theory Appl.*, vol. 48, no. 12, pp. 1510-1519, Dec. 2001.

[21] G. Cai, Y. Fang, G. Han, "Design of an adaptive multiresolution M-ary DCSK system," *IEEE Commun. Lett.*, vol. 17, no. 1, pp. 60-63, Jan. 2017.

[22] G. Cai, Y. Fang, G. Han, F. C. M. Lau, and L. Wang, "A square-constellation-based M-ary DCSK sommunication system," *IEEE Access*, vol. 4, pp. 6295-6303, 2016.

[23] G. Cai, Y. Fang, G. Han, L. Wang, and G. Chen, "A new hierarchical M-ary DCSK system: Design and analysis," *IEEE Access*, vol. 5, no. 1, pp. 17414-17424, Dec. 2017.

[24] W. Xu, L. Wang, and G. Kolumbán, "A novel differential chaos shift keying modulation scheme," *Int. J. Bifurcation Chaos*, vol. 21, no. 3, pp. 799-814, 2011.

[25] W. Xu, L. Wang, and G. Kolumbán, "A new data rate adaption communications scheme for code-shifted differential chaos shift keying modulation," *Int. J. Bifurcation Chaos*, vol. 22, no. 8, pp. 1-8, 2012.

[26] H. Yang, W. K. Tang, G. Chen, and G.-P. Jiang, "System design and performance analysis of orthogonal multi-level differential chaos shift keying modulation scheme," *IEEE Trans. Circuits Syst. I, Reg. Papers*, vol. 63, no. 1, pp. 146-156, Jan. 2016.

[27] G. Kaddoum and E. Soujeri, "NR-DCSK: A noise reduction differential chaos shift keying system," *IEEE Trans. Circuits Syst. II, Exp. Briefs*, vol. 63, no. 7, pp. 648-652, July 2016.

[28] E. Başar, Ü. Aygölü, E. Panayırcı and H. V. Poor, "Orthogonal frequency division multiplexing with index modulation," *IEEE Trans. Signal Process.*, vol. 61, no. 22, pp. 5536-5549, Nov.15, 2013.

[29] E. Basar, M. Wen, R. Mesleh, M. Di Renzo, Y. Xiao and H. Haas, "Index modulation techniques for next-generation wireless networks," *IEEE Access*, vol. 5, pp. 16693-16746, 2017.

[30] X. Cheng, M. Zhang, M. Wen and L. Yang, "Index modulation for 5G: Striving to do more with less," *IEEE Wireless Commun.*, vol. 25, no. 2, pp. 126-132, April 2018.

[31] M. C. Gursoy, E. Basar, A. E. Pusane and T. Tugcu, "Index modulation for molecular communication via diffusion systems," *IEEE Trans. Commun.*, vol. 67, no. 5, pp. 3337-3350, May 2019.

[32] M. Herceg, L. Filipović, T. Matić and G. Kaddoum, "Inductance index modulation for human body communication systems," *IEEE Wireless Commun. Lett.*, vol. 8, no. 3, pp. 937-940, June 2019.

[33] Q. Li, M. Wen, E. Basar and F. Chen, "Index modulated OFDM spread spectrum," *IEEE Trans. Wireless Commun.*, vol. 17, no. 4, pp. 2360-2374, April 2018.

[34] F. J. Escribano, A. Wagemakers, G. Kaddoum and J. V. C. Evangelista, "A spatial time-frequency hopping index modulated scheme in turbulence-free optical wireless communication channels," *IEEE Trans. Commun.*, vol. 68, no. 7, pp. 4437-4450, July 2020.

[35] G. Cai, Y. Fang, P. Chen, G. Han, G. Cai and Y. Song, "Design of an MISO-SWIPT-aided code-index modulated multi-carrier M-DCSK system for e-health IoT," *IEEE J. Sel. Areas Commun.*, doi: 10.1109/JSAC.2020.3020603.

[36] M. Wen, X. Cheng, M. Ma, B. Jiao and H. V. Poor, "On the achievable rate of OFDM with index modulation," *IEEE Trans. Signal Process.*, vol. 64, no. 8, pp. 1919-1932, Apr, 2016.

[37] G. Kaddoum, F. Richardson and F. Gagnon, "Design and analysis of a multi-carrier differential chaos shift keying communication system," *IEEE Trans. Commun.*, vol. 61, no. 8, pp. 3281-3291, August 2013.

[38] G. Cheng, L. Wang, W. Xu and G. Chen, "Carrier index differential chaos shift keying modulation," *IEEE Trans. Circuits Syst. II, Exp. Briefs*, vol. 64, no. 8, pp. 907-911, Aug. 2017.

[39] G. Cheng, L. Wang, Q. Chen and G. Chen, "Design and performance analysis of generalised carrier index M-ary differential chaos shift keying modulation," *IET Commun.*, vol. 12, no. 11, pp. 1324-1331, 17 7 2018.

[40] G. Kaddoum, M. F. A. Ahmed and Y. Nijsure, "Code index modulation: A high data rate and energy efficient communication system," *IEEE Commun. Lett.*, vol. 19, no. 2, pp. 175-178, Feb. 2015.

[41] G. Kaddoum, Y. Nijsure and H. Tran, "Generalized code index modulation technique for high-data-rate communication systems," *IEEE Trans. Veh. Technol.*, vol. 65, no. 9, pp. 7000-7009, Sept. 2016.

[42] F. Cogen, E. Aydin, N. Kabaoglu, E. Basar and H. Ilhan, "Generalized code index modulation and spatial modulation for high rate and energy-efficient MIMO systems on Rayleigh block-fading channel," *IEEE Systems Journal*. doi: 10.1109/JSYST.2020.2993704.

[43] E. Aydin, F. Cogen and E. Basar, "Code-index modulation aided quadrature spatial modulation for high-rate MIMO systems," *IEEE Trans. Veh. Tech.*, vol. 68, no. 10, pp. 10257-10261, Oct. 2019.

[44] F. Çogen, E. Aydin, N. Kabaoğlu, E. Başar and H. Ilhan, "Code index modulation and spatial modulation: A new high rate and energy efficient scheme for MIMO systems," in *2018 41st International Conference on Telecommunications and Signal Processing (TSP)*, Athens, 2018, pp. 1-4.

[45] W. Xu, Y. Tan, F. C. M. Lau and G. Kolumbán, "Design and optimization of differential chaos shift keying scheme with code index modulation," *IEEE Trans. Commun.*, vol. 66, no. 5, pp. 1970-1980, May 2018.

[46] M. Herceg, D. Vranješ, G. Kaddoum and E. Soujeri, "Permutation index DCSK modulation technique for secure multiuser high-data-rate communication systems," *IEEE Trans. Veh. Tech.*, vol. 67, no. 4, pp. 2997-3011, April 2018.

[47] M. Herceg, D. Vranješ, G. Kaddoum and E. Soujeri, "Commutation code index DCSK modulation technique for high-data-rate communication systems," *IEEE Trans. Circuits Syst. II, Exp. Briefs*, vol. 65, no. 12, pp. 1954-1958, Dec. 2018.

[48] X. Cai, W. Xu, S. Hong and L. Wang, "Dual-mode differential chaos shift keying with index modulation," *IEEE Trans. Commun.*, vol. 67, no. 9, pp. 6099-6111, Sept. 2019.

[49] G. Cai, Y. Fang, J. Wen, S. Mumtaz, Y. Song and V. Frascolla, "Multi-carrier M-ary DCSK system with code index modulation: An efficient solution for chaotic communications," *IEEE J. Sel. Topics Signal Process.*, vol. 13, no. 6, pp. 1375-1386, Oct. 2019.

[50] F. J. Escribano, A. Wagemakers, G. Kaddoum and J. V. C. Evangelista, "Design and performance analysis of an index time-frequency modulation scheme for optical communications," *IEEE J. Sel. Topics Signal Process.*, vol. 13, no. 6, pp. 1403-1416, Oct. 2019.

[51] M. Au, G. Kaddoum, M. S. Alam, E. Basar and F. Gagnon, "Joint code-frequency index modulation for IoT and multi-user communications," *IEEE J. Sel. Topics Signal Process.*, vol. 13, no. 6, pp. 1223-1236, Oct. 2019.

[52] Y. Zhou, J. Wang, and M. Sawahashi, "Downlink transmission of broadband OFCDM systems–part I: Hybrid detection," *IEEE Trans. Commun.*, vol. 53, no. 4, pp. 718-729, April 2005.

[53] Y. Zhou, T. Ng, J. Wang, K. Higuchi and M. Sawahashi, "OFCDM: A promising broadband wireless access technique," *IEEE Commun. Mag.*, vol. 46, no. 3, pp. 38-49, March 2008.

[54] Y. Zhou and T. Ng, "Performance analysis on MIMO-OFCDM systems with multi-code transmission," *IEEE Trans. Wireless Commun.*, vol. 8, no. 9, pp. 4426-4433, September 2009.

[55] X. Cai, W. Xu, D. Wang, S. Hong and L. Wang, "An M-ary orthogonal multilevel differential chaos shift keying system with code index modulation," *IEEE Trans. Commun.*, vol. 67, no. 7, pp. 4835-4847, July 2019.

[56] J. G. Proakis and M. Salehi, *Digital Communications*. New York, NY, USA: McGraw-Hill, 2007.

Xiangming Cai received the B.Sc. degree in information engineering from Guangdong University of Technology, Guangzhou, China, in 2017. He is currently pursuing the Ph.D. degree with the Department of Information and Communication Engineering, Xiamen University, Xiamen, China. His research interests include chaos-based digital communications and their applications to wireless communications.

Weikai Xu (S'10-M'12) received the B.S. degree in electronic engineering from Three Gorges College, Chongqing, China, in 2000, the M.Sc. degree in communication and information system from the Chongqing University of Posts and Telecommunications, Chongqing, China, in 2003, and the Ph.D. degree in electronic circuit and system from the Xiamen University of China, Xiamen, China, in 2011. From 2003 to 2012, he was a Teaching Assistant, and Assistant Professor with the Department of Communication Engineering, Xiamen University. He is now an Associate Professor with the department of Information and Communication Engineering, Xiamen University. His research interests include chaotic communications, underwater acoustic communications, channel coding, cooperative communications and ultra-wideband.

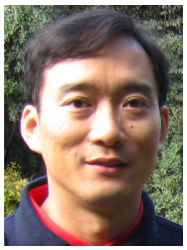

Francis C. M. Lau received the BEng(Hons) degree in electrical and electronic engineering and the PhD degree from King's College London, University of London, UK. He is a Professor at the Department of Electronic and Information Engineering, The Hong Kong Polytechnic University, Hong Kong. He is also a Fellow of IEEE and a Fellow of IET.

He is the co-author of two research monographs and a co-holder of five US patents and one pending US patent. He has published more than 300 papers. His main research interests include chaos-based digital communications, channel coding, cooperative networks, wireless sensor networks, applications of complex-network theories, and wireless communications. He was the General Co-chair of International Symposium on Turbo Codes & Iterative Information Processing (2018) and the Chair of Technical Committee on Nonlinear Circuits and Systems, IEEE Circuits and Systems Society (2012-13). He served as an associate editor for IEEE TRANSACTIONS ON CIRCUITS AND SYSTEMS II (2004-2005 and 2015-2019), IEEE TRANSACTIONS ON CIRCUITS AND SYSTEMS I (2006-2007), and IEEE CIRCUITS AND SYSTEMS MAGAZINE (2012-2015). He has been a guest associate editor of INTERNATIONAL JOURNAL AND BIFURCATION AND CHAOS since 2010.

Lin Wang (S'99-M'03-SM'09) received the M.Sc. degree in applied mathematics from the Kunming University of Technology, China, in 1988, and the Ph.D. degree in electronics engineering from the University of Electronic Science and Technology of China, China, in 2001. From 1984 to 1986, he was a Teaching Assistant with the Mathematics Department, Chongqing Normal University. From 1989 to 2002, he was a Teaching Assistant, a Lecturer, and then an Associate Professor in applied mathematics and communication engineering with the Chongqing University of Post and Telecommunication, China. From 1995 to 1996, he was with the Mathematics Department, University of New England, Armidale, NSW, Australia, for one year. In 2003, he was a Visiting Researcher with the Center for Chaos and Complexity Networks, Department of Electronic Engineering, City University of Hong Kong, for three months. In 2013, he was a Senior Visiting Researcher with the Department of ECE, University of California at Davis, Davis, CA, USA. From 2003 to 2012, he was a Full Professor and an Associate Dean with the School of Information Science and Engineering, Xiamen University, China. He has been a Distinguished Professor since 2012. He holds 14 patents in the field of physical layer in digital communications. He has authored over 100 journal and conference papers. His current research interests are in the area of channel coding, joint source and channel coding, chaos modulation, and their applications to wireless communication and storage systems.